Wiley Online Library
Early View publication on www.wileyonlinelibrary.com
(issue and page numbers not yet assigned;
citable using Digital Object Identifier – DOI)

J. Biophotonics 1–8 (2013) / DOI 10.1002/jbio.201300110

Journal of BIOPHOTONICS

FULL ARTICLE

CARS based label-free assay for assessment of drugs by monitoring lipid droplets in tumour cells

Christian Steuwe[1,3], *Imran I. Patel*[1,2,3], *Mahmud Ul-Hasan*[1,2], *Alexander Schreiner*[2], *Joan Boren*[2], *Kevin M. Brindle*[2], *Stefanie Reichelt*[2], *and Sumeet Mahajan*[*,1,3]

[1] Cavendish Laboratory, University of Cambridge, J. J. Thomson Avenue, Cambridge, CB3 0HE, UK
[2] CRUK Cambridge Research Insitute, Li Ka Shing Centre, Robinson Way, Cambridge, CB2 0RE, UK
[3] Institute of Life Sciences, University of Southampton, Highfield, Southampton, SO17 1BJ, UK

Received 5 July 2013, revised 23 August 2013, 19 October 2013, accepted 7 November 2013
Published online ■■■ ■■■ 2013

Key words: Coherent anti-Stokes Raman scattering, CARS, label-free imaging, lipid droplets, cell stress, apoptosis, drug efficiency, drug screening

Supporting information for this article is available free of charge under http://dx.doi.org/10.1002/jbio.201300110

Coherent anti-Stokes Raman scattering (CARS) is becoming an established tool for label-free multi-photon imaging based on molecule specific vibrations in the sample. The technique has proven to be particularly useful for imaging lipids, which are abundant in cells and tissues, including cytoplasmic lipid droplets (LD), which are recognized as dynamic organelles involved in many cellular functions. The increase in the number of lipid droplets in cells undergoing cell proliferation is a common feature in many neoplastic processes [1] and an increase in LD number also appears to be an early marker of drug-induced cell stress and subsequent apoptosis [3]. In this paper, a CARS-based label-free method is presented to monitor the increase in LD content in HCT116 colon tumour cells treated with the chemotherapeutic drugs Etoposide, Camptothecin and the protein kinase inhibitor Staurosporine. Using CARS, LDs can easily be distinguished from other cell components without the application of fluorescent dyes and provides a label-free non-invasive drug screening assay that could be used not only with cells and tissues *ex vivo* but potentially also *in vivo*.

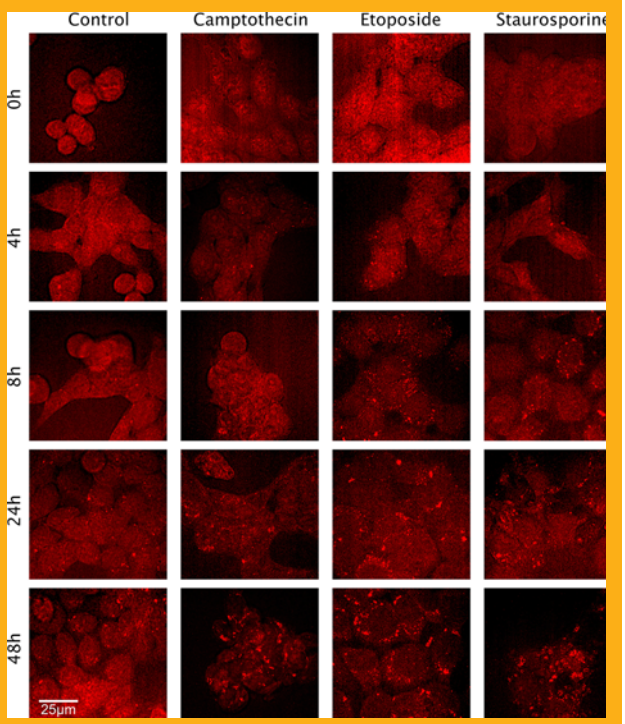

Series of CARS images of HCT 116 cells after treatment at the specified times after drug treatment.

* Corresponding author: e-mail: s.mahajan@soton.ac.uk, Phone: +44 2380593591

1. Introduction

Coherent anti-Stokes Raman spectroscopy (CARS) experienced a revival in the late nineties [2] and is now being increasingly applied for label-free bioimaging [4]. In contrast to the weak Raman scattering, where one in ten million photons is scattered inelastically, CARS utilizes a non-linear four-wave mixing process to enhance the Raman signal to enable fast imaging (pixel dwell times $<10\,\mu s$). This third order non-linear process generates blue-shifted light at the anti-Stokes frequency ω_{as} on the interaction of three photons at two different frequencies ω_s, ω_p (Figure 1A) through the third-order susceptibility ($\chi^{(3)}$) of the material. The CARS signal is spectrally separated from single photon fluorescence although it is accompanied by a non-resonant background. The latter is minimized by use of appropriate pulse duration, collection geometry and polarization-sensitive detection [4]. The CARS intensity is dependent on the cube of the input intensities:

$$I_{CARS} = N^2 I_{pump}^2 I_{Stokes} \quad (1)$$

Furthermore, the CARS signal has quadratic dependence on the number of oscillators (Raman vibration modes) N in the focal volume. Thus intense signals can be obtained for high local concentrations of vibrational oscillators; CARS of $-CH_2$ bonds in bulk sample of lipid molecules has been observed to be nine orders of magnitude stronger than their spontaneous Raman signal [5]. Moreover small molecules such as lipids, triglycerides, drugs and many other metabolites are difficult to label without loss of functionality. CARS imaging is ideally suited to provide an insight into biochemical phenomena involving such molecules.

It is for this reason that lipid metabolism, especially in the context of obesity and diseases such as diabetes and atherosclerosis, has become one of the major areas of investigation using CARS imaging, offering significant opportunities and advantages over conventional fluorescence based methods [5, 6]. For example CARS imaging has allowed study of lipid absorption in the intestine of living mice [2]; the impact of cholesterol lowering drugs in *C. elegans* [7]; helped establish the link between lipid metabolism and tumour aggressiveness [8, 9]; used to evaluate the effect of diet on formation of arterial plaques that cause thrombosis [10] and also helped unravel the chemical composition of plaques upon variation in diet [11]. Besides these demonstrations of the utility of CARS microscopy, one of the most attractive applications is the imaging of lipid droplets [12, 13], which contain exceptionally high local concentrations of lipids inside cells and tissues.

Nan et al. paved the way for live cell LD imaging and compared CARS to conventional dye based fluorescence [14]. More recently, Paar et al. observed LD growth by CARS. They demonstrated that LDs grow by transfer of lipids between individual droplets [15]. The LD composition in adipocytes and HELA cells was investigated using hyperspectral CARS microscopy and maximum entropy method to retrieve LD Raman spectra [16]. Furthermore, an emerging area of applications for CARS microscopy is the imaging of drugs and drug delivery. Apart from being able to track penetrating oil-rich ointments applied to skin [17] CARS has also been used to track deuterated drug particles in mouse tissue [18].

1.1 Lipid droplet generation and apoptosis

Cytoplasmic lipid droplets are considered to be dynamic organelles responsible not only for energy storage but many other important cellular functions. CARS imaging presents a unique opportunity to image lipids (and LDs), especially in live cells. Various studies have shown that measuring lipid quantities by applying well-known fluorescent stains such as Nile Red is unreliable as a consequence of non-specific lipid labelling, a problem that is alleviated with CARS imaging [19–21]. However, LipidTOX, a labelled phospholipid based stain, and Oil Red have been shown to be more reliable than the conventional Nile Red staining for neutral lipids [22].

LDs, which are bound by a monolayer of phospholipids, represent the major cellular storage location for neutral lipids, such as triacylglycerols (TAG) and sterol esters [23] and contain several enzymes involved in their metabolism, including enzymes responsible for lipid synthesis (acetyl-coenzyme A, acyl-COA) [24, 25] and triacylglycerol breakdown (lipases). LDs are thought to originate from the cells' endoplasmic reticulum (ER) since multiple studies [5, 26–29] suggest an association between LDs and the ER, although other investigations have shown that there is a difference between the phospholipid monolayer of LDs and the phospholipids found in the ER [30].

LDs have long been known to accumulate in tumour cells undergoing drug-induced cell death or apoptosis. ^{1}H NMR detection of the mobile lipids in these droplets has been used as a non-invasive method for detecting tumour cell death *in vivo* [31–33]. A recent study suggested that this LD accumulation is due to inhibition of fatty acid oxidation in the mitochondria, as a result of an increase in intra-mitochondrial reactive oxygen species (ROS), which diverts fatty acids away from oxidation and towards the synthesis of triacylglycerols which are the major lipid constituent of the LDs [3].

In this work we show here that CARS can be used to rapidly image the sub-cellular accumulation of LDs in tumour cells undergoing drug-induced cell death. We show that it achieves a chemical specificity for neutral lipids that is comparable to (or better than) LipidTox staining. The role of ROS in LD biogenesis was confirmed by knocking down the expression of the cytoplasmic isoform of superoxide dismutase using shRNA, which increased the number of LDs in the drug-treated cells. This study demonstrates the potential of CARS imaging to provide rapid label-free cell and tissue-based assays for measuring the time dependence and dose response to drug treatment.

2. Experimental

2.1 Compact, high power CARS laser scanning system

CARS is a 4-photon process that requires excitation by two laser beams at two different frequencies (see Figure 1A). We used a Chameleon Ultra titanium-sapphire (Ti : Sa) pulsed femtosecond laser (Coherent) split into two beams: A pump beam (835 nm) with 100 fs pulse duration and 80 MHz repetition rate and a second, Stokes beam, generated by optical parametric generation. The optical parametric oscillator (OPO) (Semi-Automatic, APE GmbH, Berlin) generates photons between 1080 nm and 1600 nm. For imaging LDs we targeted the CH_2 stretching frequency at 2845 cm^{-1}, which corresponded to the CARS frequency for neutral lipids (see Figure S3). The OPO was tuned to 1096 nm and both the beams were overlaid temporally by means of a delay stage (LTS203, Thorlabs). For spatial overlay and scanning, the galvanometer scan-head of a TriMScope (Lavision Biotec GmbH, Bielefeld, Germany) was used. By careful alignment of spatial and temporal overlay the CARS emission was optimized. For initial alignment we used highly CARS-active nanovoid samples as described earlier [34]. Pixel dwell times were <30 μs. The collinear beams were coupled into an upright microscope (BX 51, Olympus) for sample excitation and the resulting blue shifted CARS signals were read out in the Epi (back scattering) configuration. This minimized the CARS background as described in [35]. In addition we can perform multimodal imaging by using a second photomultiplier and filter set for second harmonic generation (SHG). The total power applied is less than 30 mW during imaging. A sketch including a description of the setup can be found in the supplementary material, Figure S1.

2.2 Sample preparation

A human colorectal carcinoma cell line HCT116 (ATCC, Manassas, Virginia) was grown in RPMI cell medium (Invitrogen, Carlsbad, California) supplemented with 10% Fetal Bovine Serum (Invitrogen) at 37 °C and 5% CO_2 with or without the addition of oleic acid (an unsaturated 18 carbon fatty acid that accumulates in cells and promotes LD formation). An HCT116 cell line, where expression of superoxide dismutase (SOD) had been knocked down using short hairpin RNA (shRNA) technology, was grown under the same conditions as the wild type cells. The sequence targeting expression of SOD was: GCAAAGGTGGAAATGAAGA. Decreased SOD expression was quantified using qPCR, which showed an 87 ± 4% decrease when compared to control cells.

For initial comparison between the SOD knocked-down cells, the wild type cells grown in oleic acid supplemented medium and the wild type cells grown in normal medium 5 samples for each condition were seeded on individual coverslips. Twenty four hours after seeding, Etoposide (a commonly used chemotherapeutic drug) was added to all samples. Cells were harvested at different time points after drug treatment (4 h, 8 h, 24 h, 48 h) to analyze lipid droplet formation. At each time point, cells were washed with PBS, fixed in cold 3% PFA in PBS for 1 h at 4 °C, washed three times with PBS before CARS images were acquired.

Effect of three different compounds was studied; Etoposide, Camptothecin and Staurosporine were used at 45 μM, 10 μM and 1 μM concentrations, respectively. Raman and CARS spectra of these drugs are illustrated in supplementary Figure S2 and Figure S3, respectively. Both figures show that they do not have a strong peak at 2845 cm^{-1} unlike tryacyl glycerol, which is the main component of lipid droplets. Therefore their contribution to the CARS imaging of LDs at the CH2 stretching frequency of 2845 cm^{-1} in this work is negligible. These drug concentrations were known to induce ∼50% cell death in this cell line at 24 h after drug treatment as illustrated in S1 in Boren and Brindle [3]. The control sample was treated with solvent vehicle. Similarly to the experiment described above, samples were fixed after at 0 h, 4 h, 8 h and 24 h after drug addition.

2.3 Imaging and data evaluation

A 40 × (NA: 1.2) objectives was used for CARS imaging. The colon carcinoma cells imaged here were found to be quite flat and attached very close to the glass cover-slip. Hence for consistency the fo-

cal plane ~1 μm above the glass cover-slip was chosen for imaging. A series of images was taken for each time point and each individual cell sample. Pixel dwell times of 10 to 30 μs were usually chosen depending on the CARS activity of the sample. Samples not containing a high amount of lipids required 30 μs integration time, otherwise 10 μs were sufficient. An area of 75 × 75 μm was scanned to generate highly resolved images at the optical diffraction limit with 1100 × 1100 pixels.

The lipid droplets were observed as bright spots, which were quantified using an in-house code written in MATLAB (Mathworks, UK): PMT shot noise occurring in the images was smoothed out using average filtering and the number of pixel with intensities exceeding a threshold defined by the cellular CARS background (the dispersed CARS signal from the cells) were counted. This dispersed CARS signal used as a reference for thresholding arises from the CARS signal from the distribution of lipids (and other $-CH_2$ containing bio-molecules) over the cell and primarily consists of the contribution from cell membrane. Therefore this is likely to be similar for similar cells at different timepoints. Thus although this threshold was set by manual control this did not affect the outcomes and hence, the trend observed as the cellular background provided an effective internal reference. It was raised to the point where the cell outline and internal cellular structures were no longer counted except the bright LDs.

This number was compared to the overall cell area in pixels by image segmentation. Figure S4 in the supplementary material shows unprocessed and processed MATLAB binary images and the graphical user interface used for determination of lipid droplet numbers.

2.4 Statistical analysis

Results are expressed as box and whisker plots with the box representing the median with upper and lower quartiles, whilst whiskers represent the minimum and maximum extreme values. Significant differences between median values were determined by applying the Mann Whitney test. Groups were classed as being significant if $P < 0.05$.

3. Results and discussion

Label-free CARS imaging eliminates the need for the genetically engineered tags or the stains that are used with fluorescence microscopy and avoids the

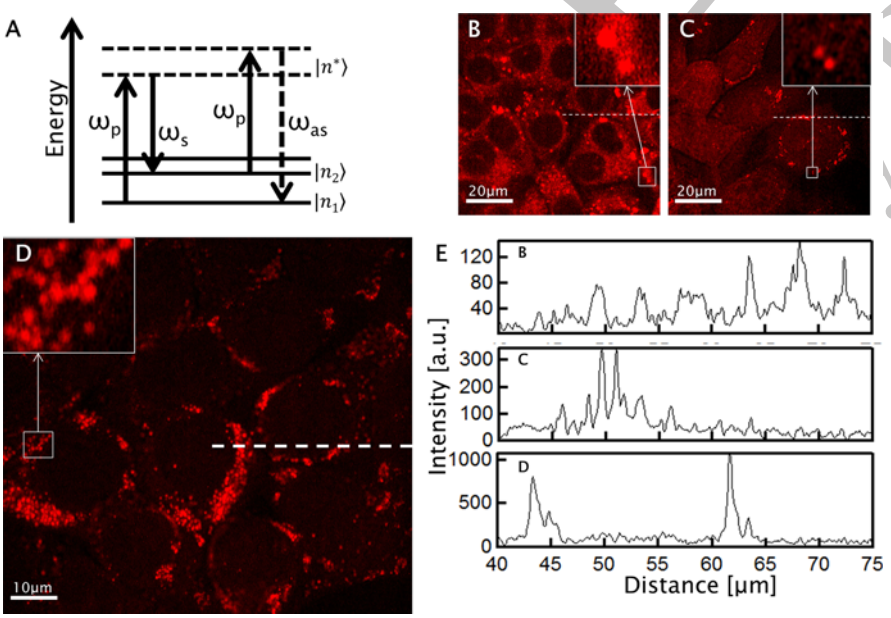

Figure 1 (**A**) An energy diagram showing the coherent anti-Stokes Raman scattering (CARS) process. The CARS photon is emitted at the anti-Stokes frequency $2\omega_p - \omega_s$. All transitions happen on a short timescale of several 100 femtoseconds to picoseconds and via short-lived virtual states n^*. (**B**) HCT116 cells 24 h after treatment with Etoposide and stained with Lipid-Tox fluorescent lipid marker. (**C**) Label-free CARS image at 2845 cm^{-1} of HCT116 cells 24 h after treatment with the Etoposide. (**D**) The same cells grown in an oleic acid rich culture medium and 24 h after treatment with Etoposide. The increased number of LDs compared to B is clearly visible. (**E**) Intensity distribution along a slice through each individual image, marked with a dashed line.

problems associated with photo-bleaching. The greatest advantage of CARS imaging is its simplicity, which we used here to evaluate the effects of different drugs via the stress-induced increase in tumour cell cytoplasmic LD content. In the first instance we compared CARS with LipidTox staining for imaging LDs.

3.1 CARS versus Fluorescence

The advantage of CARS over conventional fluorescence microscopy for imaging LDs is demonstrated in Figure 1. In CARS images of HCT cells (Figure 1C) the LDs show up as well defined areas with high intensity, which are easily distinguishable from the surrounding cytoplasm. Cells incubated with oleic acid show an even greater production of lipid droplets (Figure 1D) with greater accumulation in the cytoplasm, which is clearly distinguishable from the nucleus. In contrast, the cytoplasm of LipidTox-fluorescently stained cells (Figure 1B) show a bright background due to non-specific binding of the dye in the cytoplasm. The inset in Figure 1B shows that LDs appear as large and diffuse fluorescent areas with a reduced contrast compared to the surrounding areas. Representative line profiles for the three images (Figure 1A, B and C) are shown in Figure 1E. This shows that with CARS the lipid droplets display much sharper intensity peaks in the profiles compared to fluorescent staining, where the peaks are broader. Also the background in the fluorescent image is higher, which leads to lower contrast than in CARS.

3.2 Assessment of drug efficacy in HCT116 cells

HCT116 cells were treated with the drugs Etoposide, Camptothecin (both topoisomerase inhibitors) and Staurosporine (a protein kinase inhibitor) at con-

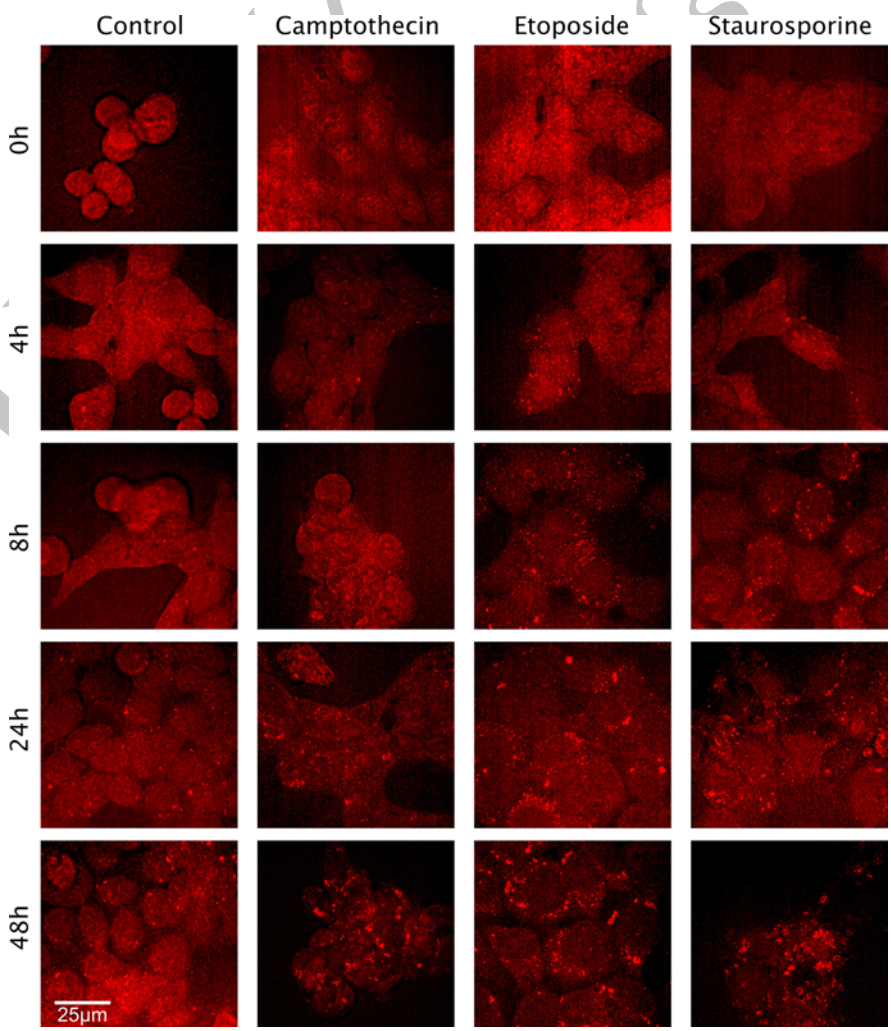

Figure 2 Series of CARS images of HCT 116 cells after treatment at the specified times after drug treatment. The increase in the number of lipid droplets (bright red spots) is clearly observed in the drug-treated samples when compared to the untreated control cells. Cells sometimes appear larger than the average cells when they are mitotic or due to a high confluence of the sample. The control images were taken with 30 µs integration time per pixel while all others are with 10 µs.

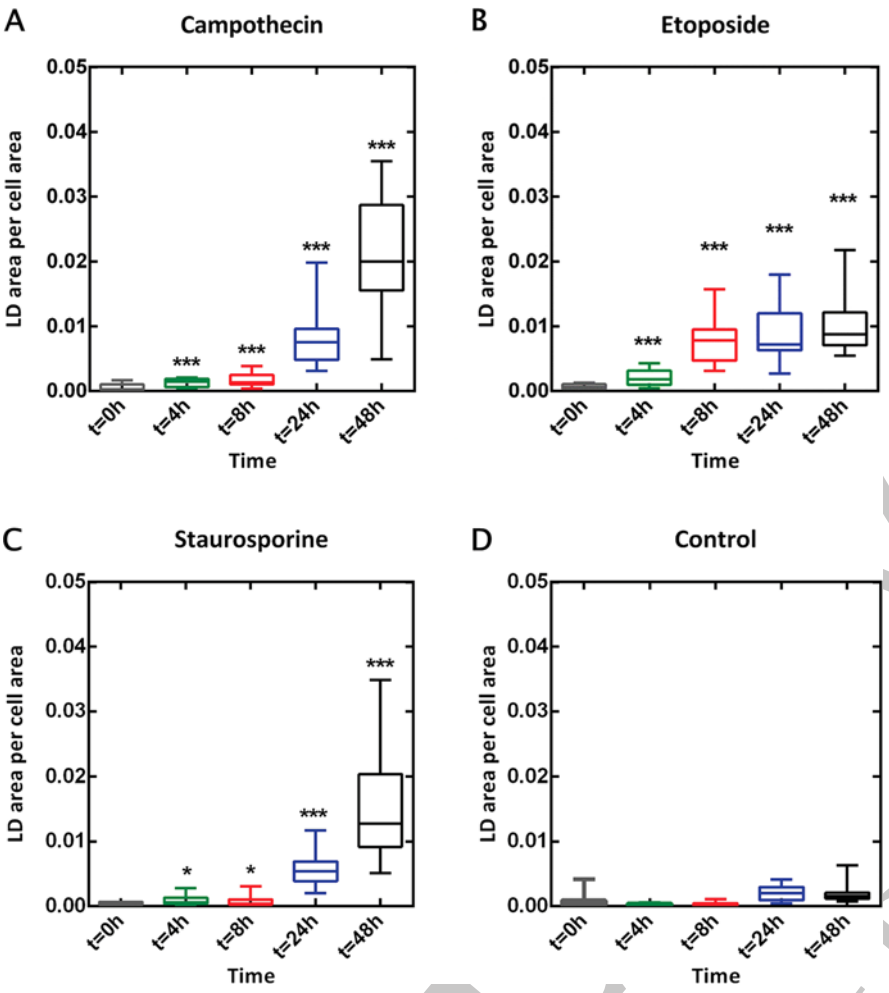

Figure 3 Drug-induced lipid droplet accumulation. HCT116 cells were treated with: (**A**) Camptothecin, (**B**) Etoposide, (**C**) Staurosporine and (**D**) control (untreated). $*p < 0.05$, $**p < 0.01$, $***p < 0.001$.

centrations previously known to induce ~50% cell death after 24 h [3]. Figure 2 shows images acquired at various time points. Compared to untreated control cells all three drugs produced a much larger increase in the number of LDs with time. The control cells showed poor contrast on imaging with CARS due to lack of lipids compared to the drug treated cells. Hence, higher pixel dwell times were used for imaging control cells compared to drug treated cells which showed increased number of lipid droplets.

Corresponding boxplots summarizing the results from approximately 150 images and 500 cells are shown in Figure 3. The LD area per unit cell area, calculated using a MATLAB script, is plotted over time. As expected, this ratio increases indicating an increase in LD generation immediately after drug treatment. In the control cells there was only a slight increase in LD content. The lipid droplet content in the drug-treated cells was significantly higher than the control cells after 8 h. Furthermore the LD numbers with the different drug treatments at each time point were significantly different from each other, as indicated by the high p-values in Figure 3, demonstrating that CARS imaging can be used to rapidly assess comparative drug efficacy.

As has been shown previously with magnetic resonance techniques [36] cells incubated with oleic acid showed significantly greater LD accumulation following treatment with etoposide when compared to cells treated with etoposide alone (Figure 4A and B). Further, in cells transfected with a vector expressing an shRNA targeted at the cytoplasmic isoform of SOD, in which the levels of SOD mRNA were decreased by 86%, there was a significantly greater accumulation of LDs (Figure 4C), which was greater than that in wild-type cells (Figure 4A). The levels of LDs after 48 h are summarized in Figure 4D, which shows that the increase in LD numbers in SOD knock-down cells were significantly greater compared to wild-type cells, confirming the role of ROS in mediating the increase in LD levels [3].

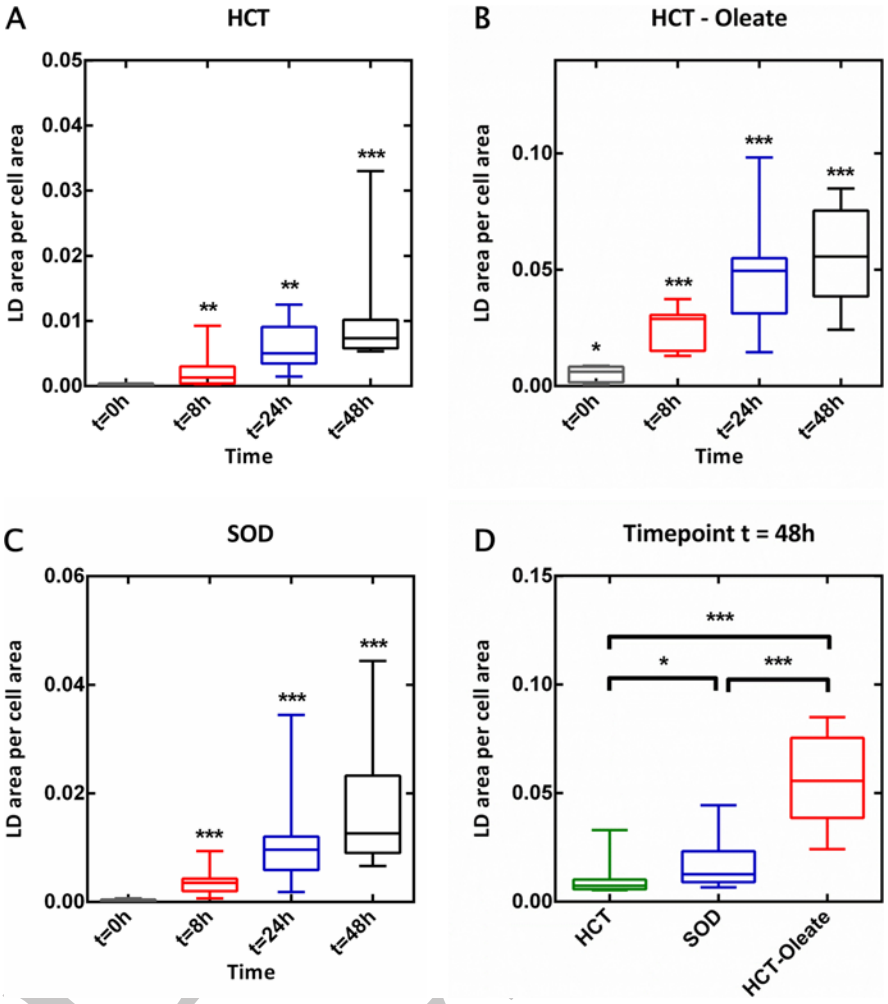

Figure 4 Boxplots showing the increased LD formation following treatment with Etoposide for (**A**) wild-type cells (**B**) wild-type cells grown with oleic acid added to the medium and (**C**) SOD knockdown cells. Cells were treated with Etoposide at 0 h. LD levels were significantly elevated in cells incubated with oleic acid. SOD knockdown cells showed higher levels of LDs when compared to the wild-type cells. Figure 4D compares the amount of LDs at a fixed timepoint for the three cases. $*P < 0.05$, $**P < 0.01$, $***P < 0.001$.

4. Conclusion

The potential of CARS microscopy for biological studies relevant to cancer and for the assessment of drug efficacy has been demonstrated with a study of the effects of different drugs on tumour cells in culture. CARS imaging of drug-induced LD accumulation showed significantly better contrast when compared with fluorescence microscopy of lipid stained cells with the LDs being clearly distinguishable from other lipids in the cytoplasm. The high levels of contrast allowed for automated analysis of LD number using simple image processing algorithms. Our CARS based assay allows assessment of efficacy of drugs by monitoring the increase in cytoplasmic LDs. It also provides confirmation of the role of ROS in the appearance of LDs on drug treatment. These results pave the way for studies of LD formation in cells and tissues *in vivo*, especially in drug-treated tumors.

Acknowledgements We acknowledge funding from EPSRC (EP/H028757/1 and EP/H028757/2), Royal Society Research Grant award (RG2011R2) and Cambridge Cancer Centre (CCC) pump-priming award for this work. We also thank the EPSRC laser loan pool. Tual Monfort is acknowledged for his help with acquiring CARS spectra.

Supplementary material Description and schematic of the setup, Raman and CARS spectra of the drugs and tripalmitoyl glycerol (a neutral lipid) and information on MATLAB evaluation are provided.

Author biographies Please see Supporting Information online.

References

[1] P. T. Bozza and J. P. Viola, Prostag. Leukot. Ess. **82**, 243–250 (2010).
[2] A. Zumbusch, G. R. Holtom and X. S. Xie, Phys. Rev. Lett. **82**, 4142–4145 (1999).

[3] J. Boren and K. M. Brindle, Cell Death Differ. **19**, 1561–1570 (2012).
[4] C. L. Evans and X. S. Xie, Annu. Rev. Anal. Chem. **1**, 883–909 (2008).
[5] H. W. Wang, Y. Fu, T. B. Huff, T. T. Le, H. Wang, and J. X. Cheng, Vib. Spectrosc. **50**, 160–167 (2009).
[6] C. Krafft, B. Dietzek, M. Schmitt, and J. Popp, J. Biomed. Opt. **17**, 040801 (2012).
[7] C. Mörck, L. Olsen, C. Kurth, A. Persson, N. J. Storm, E. Svensson, J.-O. Jansson, M. Hellqvist, A. Enejder, N. J. Faergeman, and M. Pilon, P. Natl. Acad. Sci. USA **106**, 18285–18290 (2009).
[8] J. A. Menendez and R. Lupu, Nat. Rev. Cancer **7**, 763–777 (2007).
[9] T. Migita, S. Ruiz, A. Fornari, M. Fiorentino, C. Priolo, G. Zadra, F. Inazuka, C. Grisanzio, E. Palescandolo, E. Shin, C. Fiore, W. Xie, A. L. Kung, P. G. Febbo, A. Subramanian, L. Mucci, J. Ma, S. Signoretti, M. Stampfer, W. C. Hahn, S. Finn, and M. Loda, J. Natl. Cancer I. **101**, 519–532 (2009).
[10] R. S. Lim, A. Kratzer, N. P. Barry, S. Miyazaki-Anzai, M. Miyazaki, W. W. Mantulin, M. Levi, E. O. Potma, and B. J. Tromberg, J. Lipid Res. **51**, 1729–1737 (2010).
[11] R. S. Lim, J. L. Suhalim, S. Miyazaki-Anzai, M. Miyazaki, M. Levi, E. O. Potma, and B. J. Tromberg, J. Lipid Res. **52**, 2177–2186 (2011).
[12] T. T. Le, S. Yue and J. X. Cheng, J. Lipid Res. **51**, 3091–3102 (2010).
[13] H. A. Rinia, K. N. J. Burger, M. Bonn, and M. Müller, Biophys. J. **95**, 4908–4914 (2008).
[14] X. Nan, J. X. Cheng, and X. S. Xie, J. Lipid Res. **44**, 2202–2208 (2003).
[15] M. Paar, C. Jungst, N. A. Steiner, C. Magnes, F. Sinner, D. Kolb, A. Lass, R. Zimmermann, A. Zumbusch, S. D. Kohlwein, and H. Wolinski, J. Biol. Chem. **287**, 11164–11173 (2012).
[16] M. Bonn, M. Müller, H. A. Rinia, and K. N. J. Burger, J. Raman Spectrosc. **40**, 763–769 (2009).
[17] C. L. Evans, E. O. Potma, M. Puoris'haag, D. Côté, C. P. Lin, and X. S. Xie, P. Natl. Acad. Sci. USA **102**, 16807–16812 (2005).
[18] N. L. Garrett, A. Lalatsa, I. Uchegbu, A. Schätzlein, and J. Moger, J. Biophotonics **5**, 458–468 (2012).
[19] P. Greenspan, E. P. Mayer, and S. D. Fowler, J. Cell Biol. **100**, 965–973 (1985).
[20] A. Enejder, C. Brackmann, and F. Svedberg, IEEE J. Quantum Elect. **16**, 506–515 (2010).
[21] O. Maier, V. Oberle, and D. Hoekstra, Chem. Phys. Lipids **116**, 3–18 (2002).
[22] E. J. O'Rourke, A. A. Soukas, C. E. Carr, and G. Ruvkun, Cell Metab. **10**, 430–435 (2009).
[23] Y. Guo, K. R. Cordes, R. V. Farese, and T. C. Walther, J. Cell. Sci. **122**, 749–752 (2009).
[24] L. Kuerschner, C. Moessinger, and C. Thiele, Traffic (Copenhagen, Denmark) **9**, 338–352 (2008).
[25] S. J. Stone, M. C. Levin, P. Zhou, J. Han, T. C. Walther, and R. V. Farese, J. Biol. Chem. **284**, 5352–5361 (2009).
[26] E. J. Blanchette-Mackie, N. K. Dwyer, T. Barber, R. A. Coxey, T. Takeda, C. M. Rondinone, J. L. Theodorakis, A. S. Greenberg, and C. Londos, J. Lipid Res. **36**, 1211–1226 (1995).
[27] H. Robenek, O. Hofnagel, I. Buers, M. J. Robenek, D. Troyer, and N. J. Severs, J. Cell Sci. **119**, 4215–4224 (2006).
[28] D. L. Brasaemle, J. Lipid Res. **78**, 2547–2559 (2007).
[29] N. E. Wolins, D. L. Brasaemle, and P. E. Bickel, FEBS Lett. **580**, 5484–5491 (2006).
[30] K. Tauchi-Sato, S. Ozeki, T. Houjou, R. Taguchi, and T. Fujimoto, J. Biol. Chem. **277**, 44507–44512 (2002).
[31] J. M. Hakumaki and K. M. Brindle, Trends Pharmacol. Sci. **24**, 146–149 (2003).
[32] M. Kettunen and K. Brindle, Prog. Nucl. Mag. Res. Sp. **47**, 175–185 (2005).
[33] E. J. Delikatny, S. Chawla, D. J. Leung, and H. Poptani, NMR Biomed. **24**, 592–611 (2011).
[34] C. Steuwe, C. F. Kaminski, J. J. Baumberg, and S. Mahajan, Nano Lett. **11**, 5339–5343 (2011).
[35] A. Volkmer and J. Cheng, Phys. Rev. Lett. ■■■ 87023901 (2001).
[36] R. Callies, R. M. Sri-Pathmanathan, D. Y. P. Ferguson, and K. M. Brindle, Mag. Res. Med. **29**, 546–550 (1993).

Editor's notes

Please check Ref. [13]

